Current Applied Physics 14 (2014) 1687–1691

Contents lists available at ScienceDirect

Current Applied Physics

journal homepage: www.elsevier.com/locate/cap

Spatial variation in the electronic structures of carpetlike graphene nanoribbons and sheets

Kyung-Ah Min, Dongchul Sung, Junga Ryou, Gunn Kim*, Suklyun Hong*

Department of Physics and Graphene Research Institute, Sejong University, Seoul 143-747, Republic of Korea

ARTICLE INFO

Article history:
Received 6 July 2014
Received in revised form
27 August 2014
Accepted 28 August 2014
Available online 21 September 2014

Keywords:
DFT calculations
Graphene
Graphene nanoribbon
External electric field

ABSTRACT

Graphene, when deposited on a supporting substrate with a step edge, may be deformed in the presence of the step edges of the substrate. In this study, we have investigated a spatial variation in the local electronic structure near the step region, by performing first-principles calculations for carpetlike armchair graphene nanoribbons (C-AGNR) and two-dimensional periodic carpetlike graphene sheets (PCGS). Our results indicate no practical difference in the local density of states (LDOS) between those of flat and step regions. Interestingly, however, the PCGS shows a remarkable variation in the LDOS with an external electric field (E-field). Furthermore, we also discuss the dependence of the direction and the magnitude of the applied E-field on the spatial variation in the LDOS.

1. Introduction

Because of its superior chemical and physical properties, graphene has been regarded as a promising material for the use in various applications. Various methods such as mechanical exfoliation [1,2], epitaxial growth [3], and chemical vapor deposition [4,5] can be used to produce graphene. However, from the application perspective, complete realization of the potential of graphene requires comprehensive understanding of its atomic and electronic properties, considering the complexity of many factors affecting its functionalities. This demands a concerted effort on the parts of both theory and experiment.

There are many experimental and theoretical studies concerning the atomic and electronic structures of graphene deposited on many different types of substrates. Some researchers have studied the variations in the electronic structure, in particular, those that are induced by an interaction between graphene and the substrate. For example, graphene deposited on oxide substrates such as SiO_2 and Al_2O_3 has been studied extensively [6–9]. On the other hand, many researchers observed carpetlike growth of graphene, which continuously cover the terrace and the step edge of a variety of supporting surfaces, such as SiC (0001) [10–12], Ru (0001) [13–19], Ir (111) [19–21] and Pt (111) [22,23]. Recently, it has been reported that the electronic structure of graphene on the substrate is strongly influenced by the morphology of the substrate (*e.g.* the terrace width and the step edge) [24]. Therefore, it is necessary to study the variations in the electronic structure of graphene influenced by the step edge of the supporting substrate. Although graphene structures with curvature were initially only of theoretical interest, they attract attention now with respect to a strain-based graphene engineering.

In this paper, we report an investigation of the spatial variations in the electronic structure of graphene induced by the step regions in the graphene using density functional theory (DFT). To analyze the effect of the step, we consider two types of atomic structures, namely graphene nanoribbon and graphene sheet. The local density of states (LDOS) of the flat and step regions in the two structures containing the step is analyzed to examine the dependence of the electronic structure on the external electric field (E-field). On comparing the LDOS of the flat and step regions, we show no practical difference in the electronic structure in both the models in the absence of the applied E-field. It is known that in the case of a flat graphene monolayer, its LDOS is not influenced by a uniform E-field. However, our results show a conspicuous variation in the LDOS when an E-field is applied to the step, especially in the graphene sheet. Besides, we examine the dependence of the electronic structure on the magnitude and direction of the E-field.

* Corresponding authors.
E-mail addresses: gunnkim@sejong.ac.kr (G. Kim), hong@sejong.ac.kr, suklyunh@gmail.com (S. Hong).

http://dx.doi.org/10.1016/j.cap.2014.08.025
1567-1739/

2. Computational methods and model structures

To investigate the variation in the electronic structure which is caused by the steps in graphene, we consider two types of model structures in this work. One is a carpetlike armchair graphene nanoribbon (C-AGNR) and the other is a periodic carpetlike graphene sheet (PCGS) which both consist of the flat and the step regions, as shown in Fig. 1. The unit cell contains 98 carbon atoms and 4 hydrogen atoms, passivated at the edge of the C-AGNR structure using the $N = 49$ armchair graphene nanoribbon (AGNR). On the other hand, the PCGS contained 124 carbon atoms. The width of the C-AGNR is about 60 Å while that of the PCGS is about 75 Å with a separate vacuum region of 15 Å. When graphene is adsorbed on a supporting substrate with step regions, it covers the terrace and the step edge of the substrate like a carpet on stairs. In such a situation, the electronic properties of graphene may change owing not only to the interaction with the substrate but also to the atomic structure around the step. In this work, we investigate the effect of only step regions on the electronic structure of graphene. To mimic a graphene layer formed on a substrate step, we consider the C-AGNR and the PCGS with a slope of 30°, as shown in Fig. 1. The height difference of 5 Å correspond to two atomic layer of the substrate. For example, the distances between the interlayer spacings of SiC (0001), Ru (0001), Ir (111), and Pt (111) surfaces are 2.513, 2.141, 2.216, and 2.265 Å, respectively. Taking into account the computational cost, we do not include the substrate in the simulations. Furthermore, to check the dependence of the slope, we also calculate the PCGS with a slope of 45°.

DFT calculations are performed, using generalized gradient approximation (GGA) for exchange-correlation functionals [25,26] implemented in the Vienna Ab Initio Simulation Package (VASP) [27,28]. The kinetic energy cutoff is set to 400 eV, and the electron–ion interactions are represented by projector augmented wave (PAW) potentials [29,30]. For the van der Waals (vdW) correction, we employ Grimme's DFT-D2 method [31], based on a semi-empirical GGA-type theory. For the Brillouin-zone integration, we use a $(1 \times 1 \times 1)$ grid for a C-AGNR and a $(2 \times 9 \times 1)$ grid for a PCGS, respectively, in the Gamma centered scheme for geometry optimization. For DOS calculations, $(1 \times 12 \times 1)$ and $(6 \times 20 \times 1)$ grids are utilized for the C-AGNR and the PCGS, respectively. All atomic coordinates are fully optimized, with the exception of the connecting parts of the graphene structure to satisfy the boundary condition, until all Hellmann–Feynman forces are lower than 0.05 eV/Å.

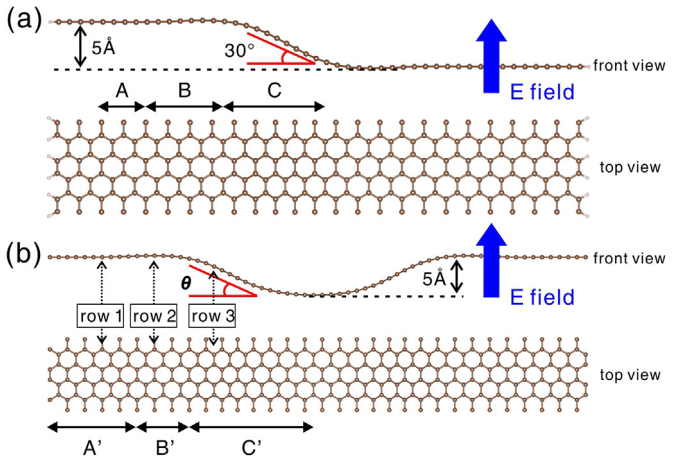

Fig. 1. Optimized structures of (a) a carpetlike armchair graphene nanoribbon (C-AGNR) and (b) a periodic carpetlike graphene sheet (PCGS) layer with a slope in step regions. In the PCGS, we consider two slopes ($\theta = 30°$ and 45°).

3. Results and discussion

3.1. Electronic structure of a carpetlike graphene nanoribbon

In the optimized C-AGNR structure, the bond lengths between neighboring carbon atoms are changed within a range −1 % to 1 % in the entire step region, compared with the C-C bond length (1.424 Å) of perfect graphene. For convenience, we divide the C-AGNR structure into three regions, as shown in Fig. 1(a). Regions A and C correspond to the flat and step regions, respectively, and region B is located in-between. In general, compression results in folding or wrinkling of graphene [32], which agrees with our result that graphene is slightly bent and a small wrinkle occurs in region B. This small wrinkle has a height of ≈ 0.19 Å.

To investigate the effect of the step, we plot the density of states (DOS) of the C-AGNR structure and compare it with that of the flat AGNR, as shown in Fig. 2(a). Black solid and red dotted curves in Fig. 2(a) represent the DOS of a flat AGNR and the C-AGNR, respectively. As seen in Fig. 2(a), there is no distinct difference between the DOS of the C-AGNR and the flat AGNR around the Fermi level (E_F), indicating the energy band gap of about 0.2 eV. This energy band gap in $N = 49$ AGNR is well matched with a previous report [33]. Therefore, we conclude that the electronic structure of the C-AGNR is not significantly affected by step regions. In Fig. 2(b), we show a calculated constant-current scanning tunneling microscope (STM) image in the Tersoff–Hamann scheme [34,35]. The method is an energy-integrated calculation of partial charge density in an energy window measured between E_F and a chosen energy E_c. For the image in Fig. 2(b), we choose $E = E_F$–0.5 eV to show the spatial variation in the charge density of the C-AGNR, compared to the flat AGNR. The calculational image of the C-AGNR is not so different from that of the flat AGNR, as expected. As in previous studies [36,37], the charge density patterns like an array of crescents are shown near the edge, which are associated with the intervalley scattering [36] of graphene due to the armchair edge.

Next, the E-field dependence of the DOS is studied by applying an E-field of magnitudes of −0.4, and 0.4 eV/Å, perpendicular to the C-AGNR. Corresponding DOS modification is analyzed with respect to the field direction. Fig. 3(a)–(c) shows the E-field dependence of the LDOS of regions A, B, and C, respectively. The blue dotted and red dashed curves represent the LDOS when the E-field of strength −0.4 and 0.4 eV/Å, respectively, is applied. For comparison, the black solid curve in Fig. 3 represents the LDOS of the C-AGNR in

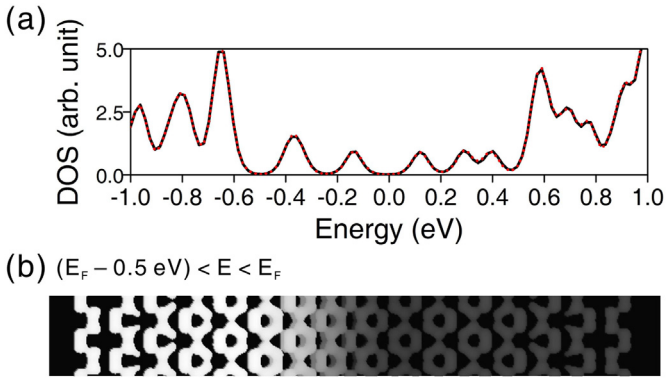

Fig. 2. (a) Density of states (DOS) for the flat armchair graphene nanoribbon (AGNR) and carpetlike armchair graphene nanoribbon (C-AGNR) with $N = 49$. Black solid and red dotted curves indicate the DOS for a perfectly flat AGNR and the C-AGNR, respectively. The Fermi level (E_F) is set to zero. (b) Simulated constant-current STM image of the C-AGNR. An energy-integrated partial charge density is calculated in an energy window between E_F–0.5 eV and E_F. (For interpretation of the references to color in this figure legend, the reader is referred to the web version of this article.)

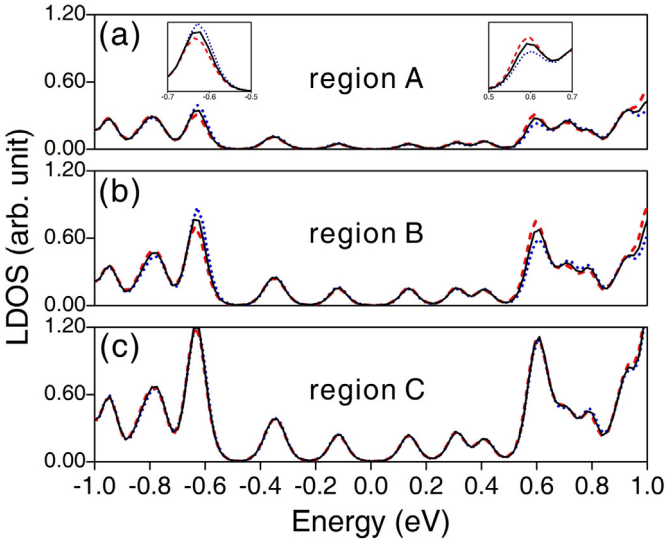

Fig. 3. Modification in the LDOS of the C-AGNR depending on the direction and magnitude of E-field. Blue dotted, black solid and red dashed curves represent the LDOS, upon applying E-fields of −0.4, 0 and 0.4 eV/Å in (a) region A, (b) region B and (c) region C, respectively. Two insets in (a) show the modification of LDOS peaks in the valence and conduction bands clearly. The Fermi level (E_F) is set to zero. (For interpretation of the references to color in this figure legend, the reader is referred to the web version of this article.)

the absence of an applied E-field. As shown in Fig. 3(c), the step region, labeled C, is relatively less affected by the E-field, compared with the other two regions (regions A and B). This could be attributed to the oblique angle of the E-field to the inclined plane. Fig. 3(a) and (b) shows small variations in the LDOS caused by energy splitting between −1.0 and −0.5 eV below the Fermi level. For the fields of −0.4 and 0.4 eV/Å, the DOS peaks move in the opposite direction. According to our calculations, modification of the DOS also occurs in the opposite manner in the energy range from 0.5 eV to 1.0 eV.

In addition, we study the dependence of modification of the DOS on the magnitude of the E-field by applying the fields of 0.4 and 0.8 eV/Å along the *z* direction. In this case, the peaks are shifted to the left and become smaller around ±0.6 eV with increasing strength of the E-field in the direction of red dashed line in Fig. 3(a) and (b). We also perform the DOS calculations for the C-AGNR by considering the increase of the E-field in the opposite direction; the peaks are shifted to the right and become higher around ±0.6 eV with increasing strength of the E-field in the blue dotted line in Fig. 3(a) and (b). Owing to the reversal of the E-field, the LDOS exhibits the opposite behavior in the energy ranges below −0.5 eV and above +0.5 eV.

3.2. Electronic structure of a periodic carpetlike graphene sheet

As mentioned above, the step has induced a small variation in the LDOS of the C-AGNR, only when E-field is applied. The dominant effect on the electronic properties originated from the ribbon edge and the oblique angle of the E-field to the incline plane. However, significant spatial variations in the electronic structure because of the curvature could be realized by considering a PCGS [see Fig. 1(b)] since it has no edge and has many wave vectors $\vec{k}$ that may be affected by the curvature of graphene. We compare the LDOS of the PCGS row by row. The LDOS of some rows demonstrates clear modification in the electronic structure. Here, we take into account two cases with slopes of 30° and 45°. In the case of PCGS with a slope of 45°, it has two small wrinkles with a height of

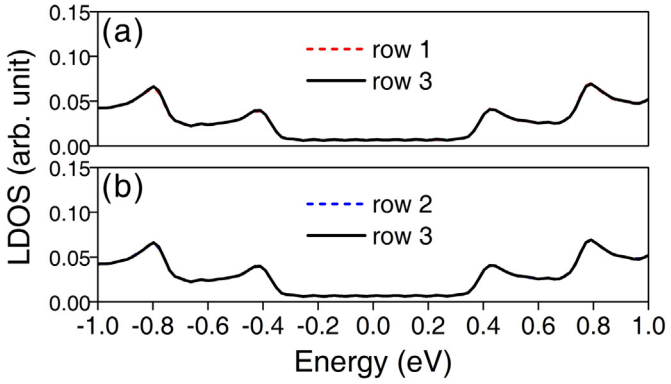

Fig. 4. LDOS for the rows in a step and two flat regions (A', B', and C' in Fig. 1(b)) in the PCGS which have a slope of 30°. The LDOS for rows 1, 2, and 3 are expressed by red dashed and blue dotted and black solid curves, respectively. The LDOS of (a) row 1 and row 3, and (b) row 2 and row 3 are shown. The Fermi level (E_F) is set to zero. (For interpretation of the references to color in this figure legend, the reader is referred to the web version of this article.)

1.34 Å, which resemble speed humps. But there is no big difference in the electronic structure between two cases (30° and 45°). Therefore, we show the LDOS of the PCGS only with the slope of 30°. Fig. 4 compares the LDOS between two rows in the flat region and a row in the step region, which are expressed by rows 1, 2, and 3 in Fig. 1(b). The LDOS of rows 1, 2, and 3 are plotted by red dashed, blue dotted and black solid curves, respectively. As in the C-AGNR, we do not find any practical difference between flat and step regions, as shown in Fig. 4.

Finally, we analyze the E-field dependence of the electronic structure of the PCGS by applying the E-field in the same manner as in the C-AGNR. Fig. 5(a) and (b) shows the LDOS of each row in the PCGS for the applied E-fields of −0.5 and +0.5 eV/Å, respectively. Black, pink and blue solid curves correspond to LDOS of each row in regions A', B' and C' as shown in Fig. 1(b), respectively. Regions A' and C' correspond to the flat and step regions, and region B' is located in-between. The field dependence is confirmed by plotting the LDOS for all rows of the PCGS. In our calculations, there is no distinct difference between the different regions in the absence of the E-field. In contrast, a striking spatial variation in the LDOS is clearly found in the ranges below −0.3 eV and above +0.3 eV in the presence of an E-field, as shown in Fig. 5. Interestingly, when the field direction is reversed, the modification pattern of the LDOS in

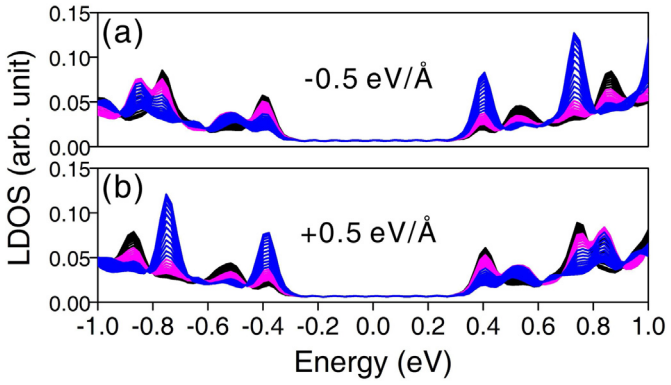

Fig. 5. Spatial variation in the LDOS for the PCGS which have a slope of 30°, upon applying the E-field of (a) −0.5 eV/Å and (b) +0.5 eV/Å. Black, pink, and blue solid curves represent the LDOS row by row in regions A', B', and C' in Fig. 1(b). The Fermi level (E_F) is set to zero. (For interpretation of the references to color in this figure legend, the reader is referred to the web version of this article.)

the valence and conduction bands is also reversed. To check whether the modification is sensitive to the supercell size, we increase the flat regions of PCGS to twice. Our results show that the spatial variation is insensitive to the supercell size.

Fig. 6(a) and (b) displays computed constant-current STM images of the PCGS with a slope of 30° for an E-field of −0.5 eV/Å. In absence of the E-field, no difference in the charge distribution of the flat and step regions could be observed. However, if an E-field is applied to the PCGS, the charge density in the step region became lower than in the flat region [Fig. 6(a)] in the energy window between E_F−0.5 eV < E < E_F. Conversely, for the energy window between $E_F < E < E_F + 0.5$ eV in Fig. 6(b), the charge density is higher in the step region than in the flat region. Inhomogeneities of the charge distribution was reported in rippled graphene monolayers on the Ru (0001) surface by using an STM experiment [38]. The spatial variation in the DOS of the graphene structures with step regions can be observed by STM experiments [21]. Fig. 6(c) shows two-dimensional map of the electric potentials of the PCGS with a slope of 45° under an applied E-field. To ensure a good representation of the total electronic potential, we choose the PCGS with a slope of 45°. One can obviously find that the potential profile has a local variation due to the presence of the step regions.

To understand the difference between the C-AGNR and the PCGS in modification of the LDOS, we terminate the boundary of the PCGS with hydrogen atoms, and change the system to a C-AGNR with the vacuum region being about 35 Å thick in the direction of the x-axis. For this model system, we do not find any substantial variation in the LDOS of the C-AGNR, depending on the external E-field. Our results show that the electronic structure of the C-AGNR is influenced mainly by the ribbon edge, whereas the PCGS is influenced by the curved structure at the step. In addition, we also consider that the PCGS has multiple $\vec{k}$ vectors in the x-axis, while C-AGNR has only one $\vec{k}$ ($\vec{k} = 0$). Therefore, some $\vec{k}$ vectors ($\vec{k} \neq 0$) may be strongly influenced by the curvature and external E-field in the PCGS.

Graphene can be corrugated by interaction with supporting substrates. The electronic structure of corrugated graphene can be influenced by changes in the distances between neighboring carbon atoms, relative rotations of the p_z orbitals, and a rehybridization between π and σ orbitals [39,40]. Such origins may give rise to weak spatial variations in our LDOS plots for the C-AGNR and the PCGS in the absence of an applied E-field. On the other hand, an external E-field gives rise to symmetry reduction to the C-AGNR and the PCGS because of the corrugation. Especially, inhomogeneity of the E-field direction is found to strongly affect the local electronic structure of the PCGS structure. In terms of electronic transport, electrical resistivity of graphene is higher as the terrace of the substrate is narrower [24]. This means that multiple scattering near the step edges is enhanced as neighboring step edges are closer.

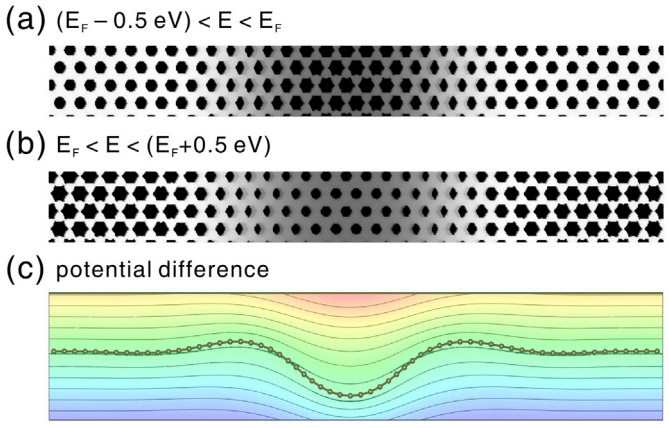

Fig. 6. Simulated constant-current STM images of the PCGS with a slope of 30° for (a) $E_c = E_F$−0.5 eV and (b) $E_c = E_F + 0.5$ eV for the E-field of −0.5 eV/Å, respectively. (c) Two-dimensional map of the electric potentials of the PCGS with a slope of 45° under an applied E-field.

4. Conclusions

In summary, the effect of step edges in carpetlike graphene sheets and nanoribbons has been investigated by using DFT calculations. In the absence of external E-field, no practical modification is found in the LDOS of the flat and step regions in both types of graphene structures (C-AGNR and PCGS). In the presence of external E-field, however, the PCGS shows a significant variation in the LDOS, whereas C-AGNR could not find a striking variation. Predicted DOS modification can be verified by the STM experiments as described above. In addition, the scanning gate microscopy technique can be considered for studying the spatial variation in the LDOS of the graphene step region. One can locally alter the electronic bands of curved graphene regions by a bias voltage from the sharp tip of an atomic force microscope, and obtains current maps corresponding to the local electronic properties.

Acknowledgments

This research was supported by Nano Material Technology Development Program (2012M3A7B4049888), the Converging Research Center Program (2013K000172), and EDISON Program (2012M3C1A6035305) through the National Research Foundation of Korea (NRF) funded by the Ministry of Science, ICT and Future Planning (MSIP), and the Priority Research Center Program (2010-0020207) through NRF funded by the Ministry of Education (MOE). G.K. acknowledges the support of the Basic Research Program (2013R1A1A2009131) of NRF/MOE.

References

[1] K.S. Novoselov, A.K. Geim, S.V. Morozov, D. Jiang, Y. Zhang, S.V. Dubonos, I.V. Grigorieva, A.A. Firsov, Science 306 (2004) 666.
[2] K.S. Novoselov, A.K. Geim, S.V. Morozov, D. Jiang, M.I. Katsnelson, I.V. Grigorieva, S.V. Dubonos, A.A. Firsov, Nature 438 (2005) 197.
[3] C. Berger, Z. Song, T. Li, X. Li, A.Y. Ogbazghi, R. Feng, Z. Dai, A.N. Marchenkov, E.H. Conrad, P.N. First, W.A. de Heer, J. Phys. Chem. B 108 (2004) 19912.
[4] K.S. Kim, Y. Zhao, H. Jang, S.Y. Lee, J.M. Kim, K.S. Kim, J.-H. Ahn, P. Kim, J.-Y. Choi, B.H. Hong, Nature 457 (2009) 706.
[5] X. Li, W. Cai, J. An, S. Kim, J. Nah, D. Yang, R. Piner, A. Velamakanni, I. Jung, E. Tutuc, S.K. Banerjee, L. Colombo, R.S. Ruoff, Science 324 (2009) 1312.
[6] A. Mattausch, O. Pankratov, Phys. Rev. Lett. 99 (2007) 076802.
[7] P. Shemella, S.K. Nayak, Appl. Phys. Lett. 94 (2009) 032101.
[8] N.T. Cuong, M. Otani, S. Okada, Phys. Rev. Lett. 106 (2011) 106801.
[9] S.M. Song, B.J. Cho, Nanotechnology 21 (2010) 335706.
[10] V. Borovikov, A. Zangwill, Phys. Rev. B 80 (2009) 121406.
[11] P. Lauffer, K.V. Emtsev, R. Graupner, Th Seyller, L. Ley, S.A. Reshanov, H.B. Weber, Phys. Rev. B 77 (2008) 155426.
[12] J. Robinson, X. Weng, K. Trumbull, R. Cavalero, M. Wetherington, E. Frantz, M. LaBella, Z. Hughes, M. Fanton, D. Snyder, ACS Nano 4 (2010) 153.
[13] J. Wintterlin, M.-L. Bocquet, Surf. Sci. 603 (2009) 1841.
[14] S. Günther, S. Dänhardt, B. Wang, M.-L. Bocquet, S. Schmitt, J. Wintterlin, Nano Lett. 11 (2011) 1895–1900.
[15] P.W. Sutter, J.-I. Flege, E.A. Sutter, Nat. Mater. 7 (2008) 406.
[16] E. Starodub, S. Maier, I. Stass, N.C. Bartelt, P.J. Feibelman, M. Salmeron, K.F. McCarty, Phys. Rev. B 80 (2009) 235422.
[17] B. Borca, F. Calleja, J.J. Hinarejos, A.L.V. de Parga, R. Miranda, J. Phys. Condens. Matter 21 (2009) 134002.
[18] S. Marchini, S. Günther, J. Wintterlin, Phys. Rev. B 76 (2007) 075429.
[19] E. Loginova, N.C. Bartelt, P.J. Feibelman, K.F. McCarty, New. J. Phys. 11 (2009) 063046.
[20] J. Coraux, A.T. N'Diaye, M. Engler, C. Busse, D. Wall, N. Buckanie, F.-J.M. zu Heringdorf, R. van Gastel, B. Poelsema, T. Michely, New. J. Phys. 11 (2009) 023006.
[21] J. Coraux, A.T. N'Diaye, C. Busse, T. Michely, Nano Lett. 8 (2008) 565.
[22] P. Sutter, J.T. Sadowski, E. Sutter, Phys. Rev. B 80 (2009) 245411.

[23] G. Otero, C. González, A.L. Pinardi, P. Merino, S. Gardonio, S. Lizzit, M. Blanco-Rey, K. Van de Ruit, C.F.J. Flipse, J. Méndez, P.L. de Andrés, J.A. Martín-Gago, Phys. Rev. Lett. 105 (2010) 216102.
[24] S.E. Bryan, Y. Yang, R. Murali, J. Phys. Chem. C 115 (2011) 10230.
[25] W. Kohn, L.J. Sham, Phys. Rev. 140 (1965) A1133.
[26] J.P. Perdew, K. Burke, M. Ernzerhof, Phys. Rev. Lett. 77 (1996) 3865.
[27] G. Kresse, J. Furthmüller, Phys. Rev. B 54 (1996) 11169.
[28] G. Kresse, J. Furthmüller, Comput. Mater. Sci. 6 (1996) 15.
[29] P.E. Blöchl, Phys. Rev. B 50 (1994) 17953.
[30] G. Kresse, D. Joubert, Phys. Rev. B 59 (1999) 1758.
[31] S. Grimme, J. Comput. Chem. 27 (2006) 1787.
[32] H. Diamant, T.A. Witten, Phys. Rev. Lett. 107 (2011) 164302.
[33] Y.-W. Son, L.C. Marvin, G.L. Steven, Phys. Rev. Lett. 97 (2006) 216803.
[34] J. Tersoff, D.R. Hamann, Phys. Rev. Lett. 50 (1983) 1998.
[35] J. Tersoff, D.R. Hamann, Phys. Rev. B 31 (1985) 805.
[36] C. Park, H. Yang, A.J. Mayne, G. Dujardin, S. Seo, Y. Kuk, J. Ihm, G. Kim, Proc. Nat. Acad. Sci. U S A 108 (2011) 18622.
[37] X. Zhang, O.V. Yazyev, J. Feng, L. Xie, C. Tao, Y.-C. Chen, L. Jiao, Z. Pedramrazi, A. Zettl, S.G. Louie, H. Dai, M.F. Crommie, ACS Nano 7 (2013) 198.
[38] A.L. Vázquez de Parga, F. Calleja, B. Borca, M.C.G. Passeggi Jr., J.J. Hinarejos, F. Guinea, R. Miranda, Phys. Rev. Lett. 100 (2008) 056807.
[39] A.H. Castro Neto, F. Guinea, N.M.R. Peres, K.S. Novoselov, A.K. Geim, Rev. Mod. Phys. 81 (2009) 109.
[40] E.-A. Kim, A.H. Castro Neto, Europhys. Lett. 84 (2008) 57007.